Effect of Sidewall Boundary Layer on a Wing in a Wind Tunnel

V. N. Vatsa*
NASA Langley Research Center, Hampton, Virginia
and
B. W. Wedan†
Vigyan Research Associates, Inc., Hampton, Virginia

Three-dimensional viscous flow calculations are performed for a swept NACA 0012 wing mounted inside a wind tunnel for which detailed experimental data are available. A Runge-Kutta time-stepping scheme is used for obtaining steady-state solutions to the thin-layer Navier-Stokes equations. The effect of the wind-tunnel sidewall boundary layer on the flow pattern over the wing surface, particularly in the vicinity of the wing/wall juncture, is found to be significant. The computed results agree well with the data over a major portion of the wing. The extent of flow separation is underpredicted on the wing, which is attributed to the use of an equilibrium turbulence model.

Introduction

THE availability of present generation supercomputers has opened the possibility of computing transonic viscous flow over realistic aircraft components. Several papers on this subject have appeared in the literature in the last two to three years.[1-3] Most of the research effort has concentrated on modeling the flow over wings and wing/body configurations, assuming that these bodies are in free air. However, the experimental data with which comparisons are made are taken inside wind tunnels where wall-interference effects can be substantial,[4] particularly in the case of solid tunnel walls. The use of wind tunnels containing ventilated and/or adaptive walls can reduce these interference effects dramatically and provide data that are nearer to freestream quality. The validity of data obtained in such tunnels for verifying numerical schemes is then improved, but may still contain interference effects that are difficult to quantify.

One way of obtaining useful data for code validation is to take measurements in a solid-wall tunnel, since such flows can be easily modeled in a computational code. Experimental studies of Lockman and Seegmiller[5] and Sobieczky et al.[6] were conducted based on such reasoning, even though it was clear that such a setup does not produce aerodynamic quality data. The data from the experimental studies of Refs. 5 and 6 have been used by various researchers for assessing the accuracy of their numerical codes.[7-9] It is believed that such code validation exercises are essential before using the computational techniques as predictive tools.

In the present study, viscous calculations using thin-layer Navier-Stokes equations are performed to simulate the flow over a NACA 0012 wing mounted on the sidewall of a solid-wall wind tunnel. The test configuration is that of Lockman and Seegmiller.[5] In the present effort, the wing-alone code of Vatsa[10] has been modified to accommodate the wind-tunnel walls as the outer boundary, with appropriate boundary conditions.

Presented as Paper 88-0102 at the AIAA 26th Aerospace Sciences Meeting, Reno, NV, Jan. 11-14, 1988; received March 28, 1988; revision received Aug. 11, 1988.

*Senior Research Scientist. Member AIAA.
†Research Engineer. Member AIAA.

Governing Equations

The basic equations under consideration here are the unsteady Navier-Stokes equations. These are specialized to a body-fitted coordinate system, ξ, η, and ζ, which represent the streamwise, spanwise, and normal coordinates, respectively. For the wing mounted inside a wind tunnel, the ζ-coordinate lines are nearly orthogonal to the wing surface and the η-coordinate lines are nearly orthogonal to the tunnel wall on which the wing is mounted. Since the dominant viscous effects for high Reynolds number turbulent flows arise from viscous diffusion normal to the body surface, a thin-layer assumption is employed here by retaining the viscous diffusion terms in both the η and ζ directions for the wind-tunnel viscous sidewall simulations. When all four tunnel walls are treated inviscidly, only the ζ-direction viscous diffusion terms are retained. The governing equations used here, therefore, constitute a more general form of the thin-layer Navier-Stokes equations than the thin-layer equation set proposed originally by Baldwin and Lomax.[11] For a coordinate system fixed in time, these equations can be written in the conservation law form as

$$\frac{\partial}{\partial t}(J^{-1}U)+\frac{\partial F}{\partial \xi}+\frac{\partial G}{\partial \eta}+\frac{\partial H}{\partial \zeta}=\frac{\partial G_v}{\partial \eta}+\frac{\partial H_v}{\partial \zeta} \tag{1}$$

where

$$U=\begin{Bmatrix}\rho\\ \rho u\\ \rho v\\ \rho w\\ \rho E\end{Bmatrix} \tag{2}$$

F, G, and H are the convective fluxes and G_v and H_v are the viscous fluxes arising because of diffusion in the η and ζ directions, respectively. The algebraic turbulence model of Baldwin and Lomax[11] is used to compute the eddy viscosity distribution for turbulent flows. The complete form of these equations is readily available in Ref. 12.

Computational Algorithm

A semidiscrete finite-volume algorithm based on Jameson's Runge-Kutta time-stepping scheme[13] is used here for obtaining steady-state solutions to the governing equations. A con-

trolled amount of dissipation is added to the present central-difference scheme to suppress odd-even decoupling and oscillations in the vicinity of shock waves and stagnation points. Although the original dissipation model proposed by Jameson et al.[13,14] is adequate for inviscid Euler equations, it is not satisfactory for Navier-Stokes computations where highly stretched meshes result from the requirement for accurate resolution of thin viscous layers. In order to obtain accurate numerical solutions on these highly stretched meshes, the isotropic dissipation model of Jameson is replaced with a nonisotropic model where the dissipation in each coordinate direction is scaled with the maximum eigenvalue of the flux Jacobian in that direction. Such scalings have also been employed by Martinelli[15] and Swanson and Turkel[16] for two-dimensional Navier-Stokes computations. In the present scheme, the dissipation is further reduced in the boundary-layer region by scaling it with the Mach number. Complete details of this dissipation model are available in Refs. 12 and 17.

Boundary Conditions

For both cases considered in this investigation, the wing surface is treated as a solid, no-slip, no-injection boundary. This condition is imposed by setting the velocity components u, v, and w to zero at the surface. An adiabatic condition is also used and the normal pressure gradient at the surface is set to zero. Similar conditions are also imposed on the wing/root tunnel sidewall in the case of the viscous sidewall simulation. For the inviscid wing/root sidewall simulation, a symmetry condition is used for all variables at the wing/root plane (sidewall) except for the crossflow velocity component, which is taken to be antisymmetric. The remaining three wind-tunnel walls are always treated as inviscid (slip) surfaces by setting the flux normal to the boundary to zero. In addition, the surface pressure is obtained by linear extrapolation from the interior. The artificial dissipation terms are set to zero at the tunnel wall boundaries, in order to prevent the introduction of mass or momentum flux into the flow from these surfaces.

The treatment of the inflow boundary is based on Riemann invariants for one-dimensional flow normal to the boundary, as discussed in detail by Jameson and Baker[14] and Thomas and Salas.[18] All variables except pressure are extrapolated at outflow. For both the viscous and inviscid sidewall simulations, the outflow pressure (back pressure) is adjusted so that the average Mach number at the inflow plane is near the experimentally determined value. An initial boundary-layer profile for the viscous wall case is specified by a 1/7 power law using a boundary-layer thickness computed by a wind-tunnel design code.[19]

Grid Generation

The grids used for these calculations are of C-O topology and are generated by a transfinite interpolation scheme[20] that allows control of the spacing normal to the wing surface and the direction of the outward grid lines. The C-type grid in the chordwise direction allows the necessary resolution in the wake region to resolve the viscous wake flow. The spanwise O-type grid wraps around the wing tip, resulting in more accurate simulation of the tip flow, which is of particular importance when the wing tip is in proximity to the wind tunnel sidewall. The C-O grid topology is illustrated in Fig. 1 for the wing in the wind tunnel. For the sake of clarity, an inviscid- rather than viscous-type grid is shown in this figure. In the case of the viscous grids, the spacing in the boundary-layer direction is approximately 10^{-5} chords to resolve the thin viscous layer, resulting in a y^+ value of approximately 6 on the wing surface for the initial grid spacing.

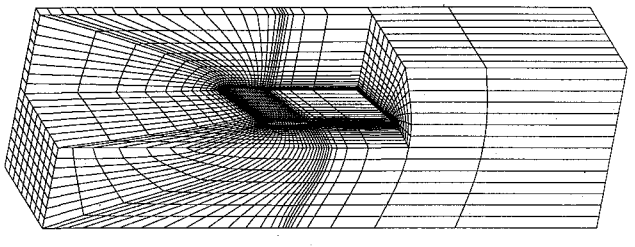

Fig. 1 Grid-topology for swept NACA 0012 wing mounted in the wind tunnel.

Results and Discussion

In this paper, an untapered, NACA 0012 wing with 20 deg sweep for which extensive data were taken by Lockman and Seegmiller[5] is considered. The wing is mounted on a sidewall in the tunnel. The wind-tunnel cross section has a small divergence angle so that the effective cross section is essentially constant after accounting for the tunnel-empty boundary-layer growth on the walls. This wall divergence is not included in the present calculations; rather, the walls are considered to be parallel since the boundary-layer development on the upper, lower, and wing-tip sidewalls is not included. As will be seen later, this resulted in less blockage than experimentally observed for the case of the inviscid sidewall simulation. The results from the viscous sidewall calculations, however, compared favorably, in a global sense, with the experimental blockage.

Viscous Sidewall Simulations

The results in the previous section indicate a discrepancy in the computed streamline patterns on the wing as compared with the experiment, although the pressures are in reasonable agreement. It is believed that these differences are a result of interaction between the wing pressures and the tunnel-sidewall boundary layer. The strong shock on the wing upper surface is sufficient to separate the sidewall boundary layer, resulting in reduced shock strength and reattachment of the wing

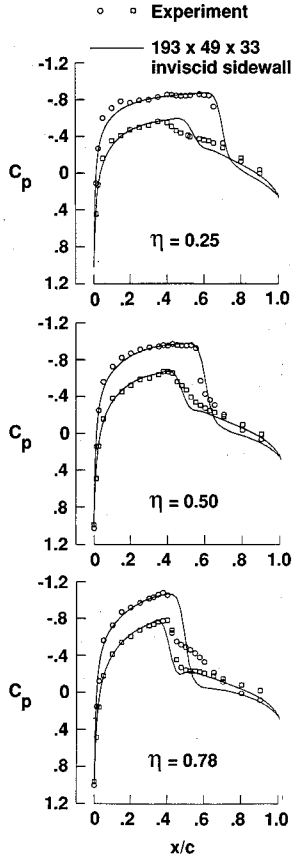

Fig. 2 Wing pressure distributions for inviscid sidewall simulation.

boundary layer in the wing/root region as seen in the experimental oil flow patterns. In order to verify this hypothesis, the capability of viscous simulation of the wing/root sidewall is included in the present code. As discussed previously, this entailed the addition of the viscous diffusion terms normal to the sidewall. The Baldwin-Lomax turbulence model used for computing the eddy viscosity for the wing-surface boundary layer is also used to obtain values of eddy viscosity resulting from the sidewall boundary layer. The local interior value of eddy viscosity used in the calculation is then obtained by combining the value from the wing and the sidewall as

$$\bar{\varepsilon} = \frac{\bar{\varepsilon}_w \ell_{sw}^2 + \bar{\varepsilon}_{sw} \ell_w^2}{\ell_w^2 + \ell_{sw}^2}$$

where $\bar{\varepsilon}_w$ and $\bar{\varepsilon}_{sw}$ are the values of eddy viscosity computed from the Baldwin-Lomax model as applied to the wing and sidewall, respectively. The lengths ℓ_w and ℓ_{sw} are the normal distances of the interior point from the wing and sidewall surfaces. This formulation has the desired property that the eddy viscosity reduces to the appropriate surface value as the distance of the interior point from the surface goes to zero.

The same approach for defining the flow conditions in the tunnel is used for this case as was used for the inviscid sidewall problem. This involved specifying the back pressure so as to obtain the desired inflow conditions. For the viscous sidewall case, it was found, however, that the inflow Mach number was highly sensitive to, and varied nonlinearly with, the back pressure. The effect on the inflow conditions of varying the back pressure was reported by the authors in Ref. 12. Based on numerical experimentation, a value of 0.975, which agrees favorably with the experimental value, was selected for the back pressure level p_b/p_∞. This value was found to give the best overall agreement with the experimental inflow conditions and was, therefore, employed in the present computations.

The Reynolds number based on chord length and freestream conditions is 8×10^6 for the case presented here. The freestream Mach number is 0.826 and the angle of attack is taken to be 2 deg to correspond to the experimental test conditions of Ref. 5. This test case has also been investigated in earlier papers by Holst et al.[7] and Kaynak and Flores.[8]

Before presenting the results, it is appropriate to mention that the numerical solutions were run until at least four orders of reduction was obtained in the magnitude of the average residuals. This was achieved in usually less than 4000 cycles for all the cases presented here. However, the numerical solutions were generally run for 5000 cycles to ascertain that key flow properties, such as surface pressures and surface streamline patterns, had reached a converged state.

Inviscid Sidewall Simulations

The first test problem considered in this section assumes all the tunnel walls to be inviscid and, hence, the effect of boundary layers developing on the tunnel walls is neglected in this section. An analysis of artificial dissipation and grid density effects for this problem were reported by the authors in Ref. 12. Based on this work, a grid consisting of $193 \times 49 \times 33$ mesh points in the streamwise, normal, and spanwise directions, respectively, is employed here. As was pointed out in Ref. 12, effects of grid density are minimal on such a mesh for this problem.

The sectional pressure distributions from these calculations are compared with the experimental data in Fig. 2. The predicted shock positions on the upper surface at 25 and 50% span locations agree fairly well with the data. On the lower surface of the inboard station, the computed solutions indicate a stronger shock than observed experimentally. It is believed that this is caused by ignoring the boundary layer developing on the sidewall in these calculations. The agreement at the 78% span station is not entirely satisfactory, since the experimentally observed pressure plateau on the upper surface is not seen in the numerical results. This is due to the underprediction of the reverse flow region on the upper surface of the wing. Since we are using an equilibrium turbulence model (namely, the Baldwin-Lomax turbulence model), it is not surprising to find this to be the case.

The experimental streamline pattern of Ref. 5 indicates that the reverse flow zone does not extend all the way to the wing/root juncture. The computed surface streamlines shown in Fig. 3, however, indicate that this reverse flow region extends from the tunnel wall out to the 85% span station. The corresponding pressure contours (Fig. 4) indicate that the shock strength is undiminished up to the wing/root wall, as would be expected from the inviscid treatment of the sidewall. This strong shock in the wing/root region is sufficient to cause the separated region to extend to the wing/root tunnel sidewall.

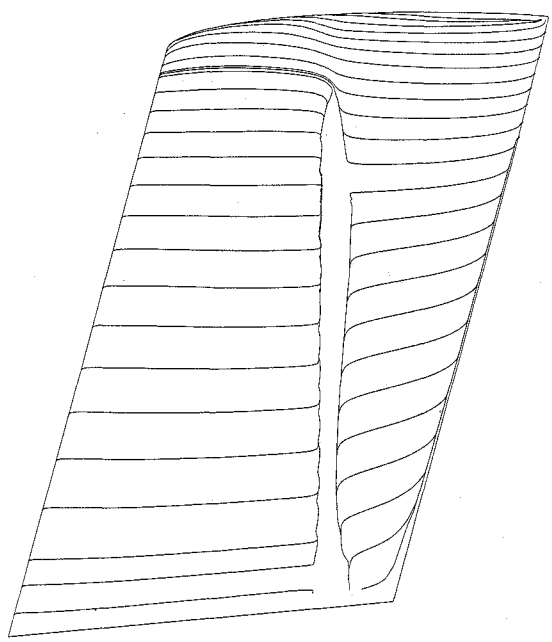

Fig. 3 Streamline pattern on the upper surface of wing for inviscid sidewall simulation.

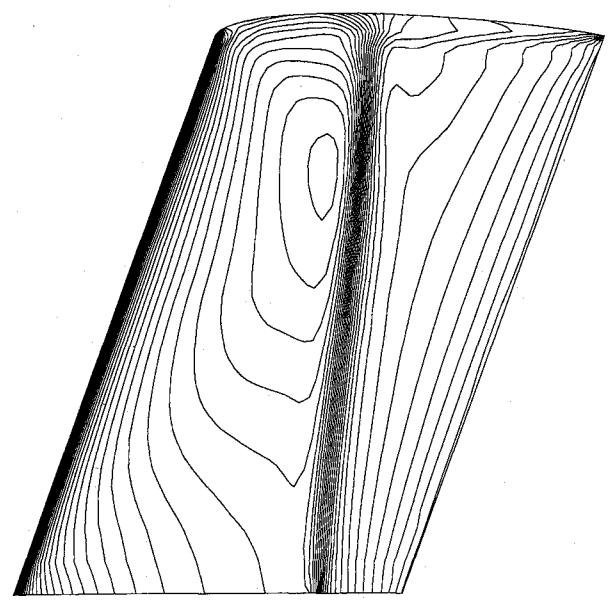

Fig. 4 Pressure contours on upper surface of wing for inviscid sidewall simulation.

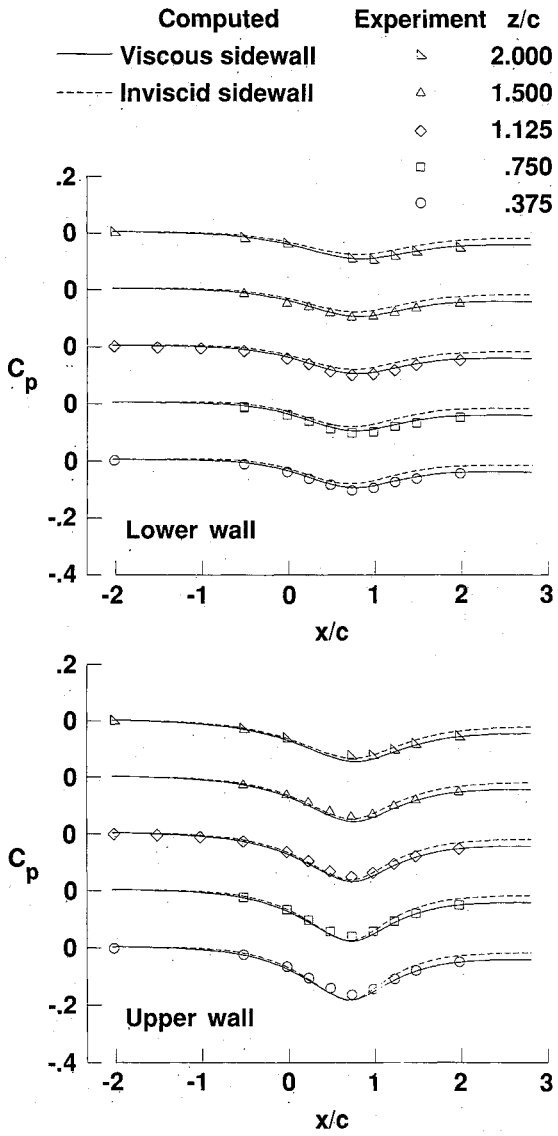

Fig. 5 Upper and lower tunnel-wall pressure distributions.

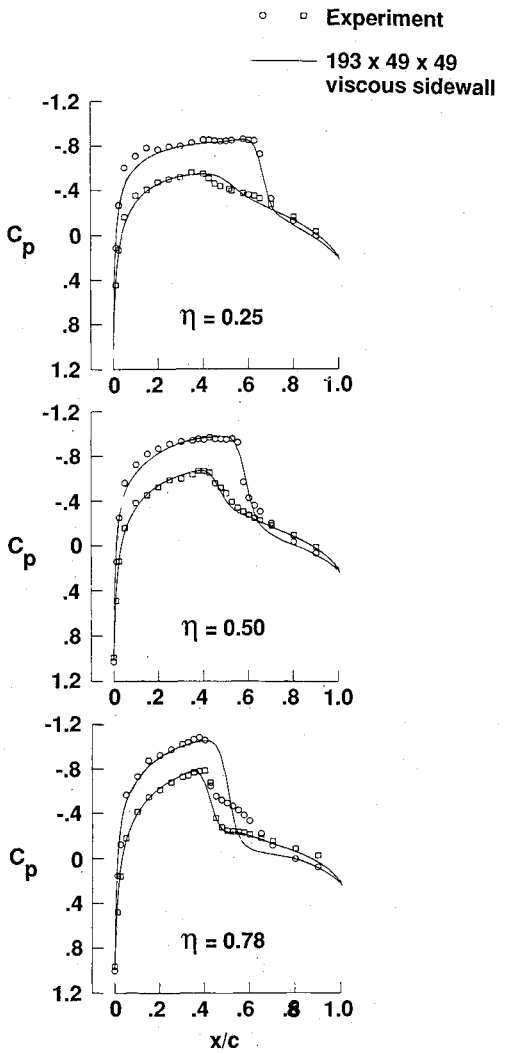

Fig. 6 Wing pressure distributions for viscous sidewall simulation.

The resulting solutions are compared with the experimental data in Fig. 5 for the tunnel-wall pressures and in Fig. 6 for the wing-surface pressures. In Fig. 5, the results from the inviscid sidewall simulation are also presented. The inviscid sidewall solutions display higher back pressure levels than the data, indicating less overall tunnel blockage than observed experimentally. The solutions from the viscous sidewall simulations agree reasonably well with the data. These results clearly demonstrate the need for including the boundary-layer growth on the sidewall for accurate prediction of tunnel blockage.

The sectional pressure distributions shown in Fig. 6 compare well with the experimental data at 25 and 50% span stations. The lower surface pressure distributions show significant improvement over the inviscid sidewall simulation results. It appears that the shock strength near the inboard span stations on the wing surface is reduced due to the interaction with the sidewall boundary layer, resulting in improved agreement with the data.

The pressure contours for the viscous sidewall case are shown in Fig. 7 for the upper surface of the wing. The weakening of the wing-surface shock strength toward the wing/root junction is clearly visible in this figure. The corresponding streamline pattern in Fig. 8 shows that the reverse flow does not extend all the way to the wing/root region. The streamlines in the wing/root region are displaced outward in

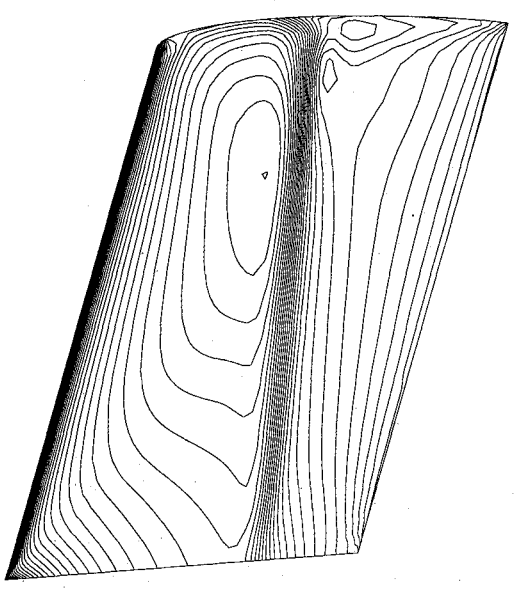

Fig. 7 Pressure contours on the upper surface of wing for viscous sidewall simulation.

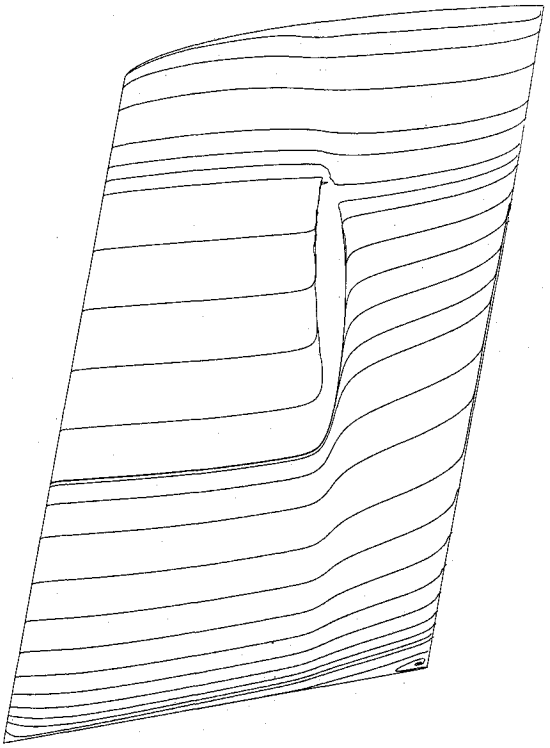

Fig. 8 Streamline pattern on the upper surface of wing for viscous sidewall simulation.

the spanwise direction due to the boundary layer developing on the tunnel wall. These solutions display the correct physical behavior in the wing/root region and compare much better with the experimental data. Even though the computed pressures compare well with the experimental data over a major portion of the wing, the extent of the streamwise separation, particularly in the outboard region, is still underpredicted. This is attributed to the fact that the equilibrium turbulence model employed here is inadequate for predicting flows with large reverse flow regions.

Concluding Remarks

Detailed viscous calculations are presented for a swept NACA 0012 wing mounted inside a solid-wall wind tunnel under transonic flow conditions. The boundary-layer interaction in the corner region formed by the tunnel wall and the wing surface has significant effect on the flow pattern on the wing surface near the root plane. Based on the present results, it appears that, for accurate prediction of flow over the wing, it is essential to account for the boundary-layer growth on the tunnel wall on which the wing is mounted. Finally, it should be pointed out that the present computations using an equilibrium turbulence model (Baldwin-Lomax) underpredict the extent of streamwise separation on the upper surface of the wing. It is anticipated that incorporation of a nonequilibrium turbulence model in the present code would improve the predictions of flows with large separated flow regions.

Acknowledgments

The authors are deeply indebted to Dr. J. L. Thomas of the Analytical Methods Branch for many stimulating discussions throughout the course of this study. The authors would also like to thank Dr. E. C. Anderson of the Theoretical Aerodynamics Branch for his computations of the initial boundary-layer profiles used in obtaining the viscous wall results and Dr. P. A. Newman for sharing with us some of his knowledge of the physical nature of flow in a wind tunnel under transonic conditions.

References

[1]Fuji, K., "Navier-Stokes Simulation of Transonic Flow over Wing-Fuselage Combinations," AIAA Paper 86-1831, June 1986.

[2]Thomas, J. L., Taylor, S. L., and Anderson, W. K., "Navier-Stokes Computations of Vortical Flows Over Low Aspect-Ratio Wings," AIAA Paper 87-0207, Jan. 1987.

[3]Deese, J. E. and Agarwal, R. K., "Navier-Stokes Calculations of Transonic Viscous Flow About Wing-Body Configurations," AIAA Paper 87-1200, June 1987.

[4]Pindzola, M. and Lo, C. F., "Boundary Interference at Subsonic Speeds in Wind Tunnels with Ventilated Walls," Arnold Engineering Development Center, TR-69-47, 1969.

[5]Lockman, W. K. and Seegmiller, H. L., "An Experimental Investigation of the Subcritical and Supercritical Flow About a Swept Semispan Wing," NASA TM 84367, June 1983.

[6]Sobieczky, H., Hefer, G., and Tusche, S., "DFVLR-F5 Test Wing Experiment for Computational Aerodynamics," *Proceedings of the AIAA 5th Applied Aerodynamics Conference*, AIAA, New York, 1987.

[7]Holst, T. L., Gundy, K. L., Flores, J., and Chaderjian, N. M., "Numerical Solution of Transonic Wing Flows Using an Euler/Navier-Stokes Zonal Approach," AIAA Paper 85-1640, June 1985.

[8]Kaynak, U. and Flores, J., "Advances in the Computation of Transonic Separated Flows over Finite Wings," AIAA Paper 87-1195, June 1987.

[9]Kordulla, W. (ed.), "Numerical Simulation of the Transonic DFVLR-F5 Wing Experiment—Towards the Validation of Viscous Wing Flow Codes," *Proceedings Notes on Numerical Fluid Mechanics*, Vol. 22, Vieweg Verlag, Braunschweig, FRG, 1988.

[10]Vatsa, V. N., "Accurate Numerical Solutions for Transonic Viscous Flow Over Finite Wings," *Journal of Aircraft*, Vol. 24, June 1987, pp. 377–385.

[11]Baldwin, B. S. and Lomax, H., "Thin Layer Approximation and Algebraic Model for Separated Turbulent Flows," AIAA Paper 78-257, Jan. 1978.

[12]Vatsa, V. N. and Wedan, B. W., "Navier-Stokes Solutions for Transonic Flow Over a Wing Mounted in a Tunnel," AIAA Paper 88-0102, Jan. 1988.

[13]Jameson, A., Schmidt, W., and Turkel, E., "Numerical Solutions of the Euler Equations by Finite Volume Methods Using Runge-Kutta Time-Stepping Schemes," AIAA Paper 81-1259, June 1981.

[14]Jameson, A. and Baker, T. J., "Solution of the Euler Equations for Complex Configurations," AIAA Paper 83-1929, June 1983.

[15]Martinelli, L., "Calculation of Viscous Flows with Multigrid Methods," Ph. D. Dissertation, Mechanical & Aerospace Engineering Dept., Princeton Univ., Princeton, NJ, 1987.

[16]Swanson, R. C. and Turkel, E., "Artificial Dissipation and Central Difference Schemes for the Euler and Navier-Stokes Equations," AIAA Paper 87-1107, June 1987.

[17]Vatsa, V. N., Thomas, J. L., and Wedan, B. W., "Navier-Stokes Computations of Prolate Spheroids at Angle of Attack," *Proceedings of the AIAA Atmospheric Flight Conference*, AIAA, New York, 1987.

[18]Thomas, J. L. and Salas, M. D., "Far-Field Boundary Conditions for Transonic Lifting Solutions to the Euler Equations," AIAA Paper 85-0020, Jan. 1985.

[19]Anderson, E. C. and Lewis, C. H., "Laminar or Turbulent Boundary-Layer Flows of Perfect Gases or Reacting Gas Mixtures in Chemical Equilibrium," NASA CR-1893, 1971.

[20]Eriksson, L. E., "Transfinite Mesh Generation and Computer-Aided Analysis of Mesh Effects," Ph.D. Dissertation, Uppsala Univ., Uppsala, Sweden, March 1984.